

Neural Collapse-Inspired Multi-Label Federated Learning under Label-Distribution Skew

Can Peng¹, Yuyuan Liu¹, Yingyu Yang¹, Prमित Saha¹, Qianye Yang¹, J. Alison Noble¹

¹University of Oxford, Oxford, United Kingdom

Abstract

Federated Learning (FL) enables collaborative model training across distributed clients while preserving data privacy. However, the performance of deep learning often deteriorates in FL due to decentralized and heterogeneous data. This challenge is further amplified in multi-label scenarios, where data exhibit complex characteristics such as label co-occurrence, inter-label dependency, and discrepancies between local and global label relationships. While most existing FL research primarily focuses on single-label classification, many real-world applications, particularly in domains such as medical imaging, often involve multi-label settings. In this paper, we address this important yet underexplored scenario in FL, where clients hold multi-label data with skewed label distributions. Neural Collapse (NC) describes a geometric structure in the latent feature space where features of each class collapse to their class mean with vanishing intra-class variance, and the class means form a maximally separated configuration. Motivated by this theory, we propose a method to align feature distributions across clients and to learn high-quality, well-clustered representations. To make the NC-structure applicable to multi-label settings, where image-level features may contain multiple semantic concepts, we introduce a feature disentanglement module that extracts semantically specific features. The clustering of these disentangled class-wise features is guided by a predefined shared NC structure, which mitigates potential conflicts between client models due to diverse local data distributions. In addition, we design regularisation losses to encourage compact clustering in the latent feature space. Experiments conducted on four benchmark datasets across eight diverse settings demonstrate that our approach outperforms existing methods, validating its effectiveness in this challenging FL scenario.

Introduction

Federated Learning (FL) has emerged as a promising framework for analysing sensitive data, particularly in domains like healthcare imaging, where privacy and legal constraints prevent direct data sharing. However, most existing FL approaches are limited to basic multi-class classification tasks, failing to account for more realistic scenarios where multiple labels frequently co-occur within a single sample. For

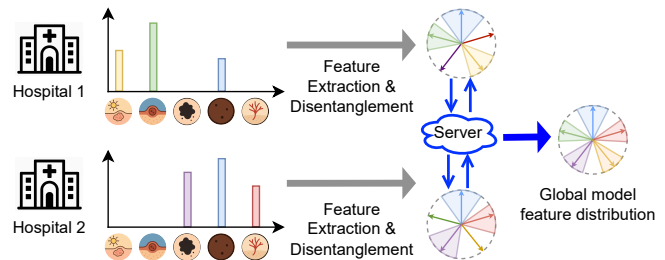


Figure 1: Within an FL system, clients may present distinct data distributions and label relationships. For example, Client 1 primarily serves patients with sun exposure-related skin lesions, whereas Client 2 mainly handles cases involving melanoma and vascular lesions. The proposed method aims to address multi-label, label-skewed FL scenarios by disentangling class-specific features and promoting structured feature clustering in the latent feature space.

instance, many diseases are interrelated, and patients often present with multiple conditions or symptoms simultaneously, rather than a single isolated issue. This multi-label nature of real-world data is often overlooked. Another core challenge in FL is data heterogeneity across clients, as each client (e.g., hospital) may possess a uniquely skewed data distribution. This variation arises from differences in geography, population demographics, medical facilities, and clinical expertise. As a result, clients may exhibit label imbalance, including majority, minority, or even missing (vacant) classes. Under multi-label scenarios, such heterogeneity becomes even more pronounced, making collaboration across clients significantly more difficult. Figure 1 illustrates this scenario, demonstrating that hospitals may hold datasets containing various sets of dermatological conditions.

In this paper, we explore the problem of multi-label FL under label-skewed conditions, where each client’s local data is both imbalanced and divergent from the global distribution. Without directly sharing local data, the goal is to collaboratively train a global model that performs well across all target classes, despite the presence of class imbalance and missing labels on certain clients. To tackle the unique challenges posed by multi-label, label-skewed FL, we propose a novel method called Federated Neural Collapse Alignment for Multi-Label

Learning (FedNCAlign-ML). Our approach introduces a representation learning framework for multi-label FL, inspired by Neural Collapse (NC) theory (Papayan et al., 2020), to enhance feature alignment across clients with heterogeneous label distributions. Specifically, we first encode each input image using a standard feature extractor, producing an image-level representation potentially containing multiple semantic concepts. We then leverage attention mechanisms to extract class-specific representations from this image-level representation, generating disentangled, class-wise embeddings. This effectively decomposes the complex multi-label problem into multiple single-label problems. Next, motivated by the NC phenomenon, we incorporate a predefined Equiangular Tight Frame (ETF) structure to promote consistent and discriminative feature alignment across clients, even under non-IID data distributions. The ETF structure facilitates class-independent clustering, encouraging local models to align with the global class geometry rather than overfitting to their local data distributions. Additionally, we introduce two complementary regularisation terms to enhance feature clustering in the latent feature space. A rejection loss filters out noisy signals from negative features, and a contrastive loss encourages compact intra-class clustering and clear inter-class separation. The key contributions of this paper are as follows:

- We explore the important yet underexplored problem of multi-label FL under label-skewed conditions. To this end, we propose FedNCAlign-ML, a novel method inspired by Neural Collapse theory.
- FedNCAlign-ML effectively adapts established representation learning techniques from the multi-class to the multi-label setting, and tackles the challenges introduced by heterogeneous local data distributions, label co-occurrence, and inter-label dependency.
- To handle the presence of multiple semantic concepts within multi-label samples, we introduce an attention-based feature disentanglement block that extracts class-specific representations from image-level features. Additionally, we incorporate two regularisation terms, one to suppress noisy negative features and another to promote compact class-wise clustering.
- We evaluate the proposed FedNCAlign-ML method on four benchmark datasets under eight diverse settings, comparing it to state-of-the-art FL approaches. The results show that FedNCAlign-ML consistently outperforms existing methods, achieving improvements of up to 2.87% in class-wise AUC and 7.29% in class-wise F1 score.

Related Work

Heterogeneous Federated Learning

The foundational FL algorithm, FedAvg (McMahan et al., 2017), performs iterative weighted averaging of locally trained model parameters. This process involves local training on

client devices, aggregation at a central server, and broadcasting the updated global model back to clients. While FedAvg performs well under independently and identically distributed (IID) data, real-world scenarios often involve non-IID data distributions. These distributions are commonly observed as quantity skew, label distribution skew, and feature distribution skew, all of which present significant challenges for FL. In the context of multi-class classification, numerous methods have been proposed to address such data heterogeneity within FL settings. For instance, FedProx (Li et al., 2020) adds an L2 regularisation term to constrain local updates and encourage proximity to the global model. FedCurv (Shoham et al., 2019) uses Elastic Weight Consolidation (Kirkpatrick et al., 2017) to preserve important local parameters to reduce divergence across clients. SCAFFOLD (Karimireddy et al., 2020) introduces control variates to correct client drift. SphereFed (Dong et al., 2022) projects features onto a hypersphere using a fixed classifier to mitigate latent feature distribution discrepancies. FedVLS (Guo et al., 2025) applies global model distillation to alleviate forgetting of missing classes and regularisation to amplify minority class losses, thereby improving performance on underrepresented classes. Although these approaches have demonstrated effectiveness in the multi-class setting, their performance tends to deteriorate when directly applied to the more complex multi-label scenario, where each sample may be associated with multiple co-occurring labels. In this work, we focus on addressing the challenges of multi-label FL under quantity-skewed and label-skewed data distribution.

Multi-Label Federated Learning

Although multi-label classification is a fundamental task, it remains less explored than multi-class classification in image processing. In the context of FL, the multi-label setting introduces additional and distinct challenges compared to the multi-class scenario, including label co-occurrence, inter-label dependency, and divergence between local and global label relationships. FedLGT (Liu et al., 2024) addresses these challenges by focusing on modelling label correlations across clients. Building upon C-Tran (Lanchantin et al., 2021), it leverages frozen CLIP (Radford et al., 2021) text embeddings to maintain consistent label relationships and reduce divergence in label dependencies among clients. In contrast, our approach focuses on understanding the structure of the latent feature space and explicitly controlling and optimising it to enhance robustness under challenging label-skewed FL conditions.

Neural Collapse-Inspired Methods

Recent research has shown that during the terminal phase of training (TPT), a phenomenon known as Neural Collapse (NC) emerges (Papayan et al., 2020). TPT refers to the stage when overparameterized deep networks are trained on balanced multi-class classification datasets, and the model’s performance plateaus while the training loss remains non-zero and continues to decrease. NC describes a distinctive geomet-

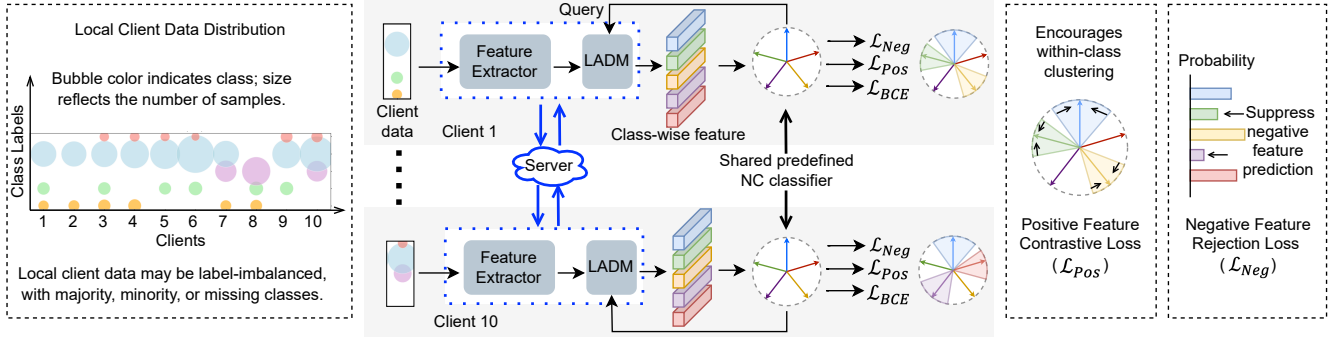


Figure 2: Framework for the proposed FedNCAAlign-ML method for addressing multi-label, label-skewed FL. First, an attention-based Label-Aware Disentanglement Module (LADM) extracts label-specific features from image-level representations. Then, a predefined ETF matrix serves as both the shared classifier and the source of class-wise query embeddings, enabling consistent local training across clients. Additionally, two regularisation terms are introduced to suppress noisy negative features and encourage compact intra-class clustering in the latent feature space.

ric structure in the latent feature space: final-layer features collapse to their corresponding within-class means, and these class-wise prototypes align to form the vertices of a simplex Equiangular Tight Frame (ETF). As this simple yet elegant mathematical structure provides an optimal linear separable state for classification, NC-inspired classifiers have been explored in various domains, including federated learning (Li et al., 2023b), incremental learning (Yang et al., 2023b; Wei et al., 2025), few-shot learning (Yang et al., 2023b), and long-tail recognition (Gao et al., 2024). Despite growing interest, most existing work has focused on multi-class classification, while the equally important challenge of multi-label classification remains underexplored. To address this gap, Li et al. (2023a) investigates the presence of NC in multi-label settings. They find that network training on a balanced multi-label dataset also exhibits NC but in a generalised form. In particular, features corresponding to single-label instances still conform to the Simplex ETF structure, while features associated with multi-label instances tend to approximate scaled averages of the single-label prototypes. MLC-NC (Tao et al., 2025) uses NC to process the long-tailed multi-label classification task in a centralised setting. However, it does not consider the missing class condition, which frequently arises in label-skewed FL scenarios across individual clients. To the best of our knowledge, our paper is the first to explore multi-label FL from an NC perspective. It opens the possibility to solve the heterogeneous multi-label FL challenge by fundamentally avoiding interference due to various local data distributions, label co-occurrence, and inter-label dependency.

Preliminaries

Problem Formulation

In a multi-label, label-skewed FL setting, a total of K clients collaboratively train a shared global model. Each client k has a local dataset $D_k = \{(x_i^k, y_i^k)\}_{i=1}^{N_k}$, containing N_k sam-

ples. Each sample (x_i^k, y_i^k) consists of an input image $x_i^k \in \mathbb{R}^{W \times H \times 3}$ and a corresponding multi-hot label vector $y_i^k \in \mathbb{R}^C$, indicating the presence of one or more of the C possible classes in the image. Due to the label-skewed nature of the scenarios, each client may only have access to a subset of the total class set, denoted as $C_k \subseteq C$. Moreover, even for the present classes, the data distribution may differ significantly across clients. The objective of the federated system is to learn a global model that can accurately recognise all C classes, without requiring clients to share their local data.

Neural Collapse

In this section, we first introduce the structure of the simplex ETF, followed by a discussion of the key properties of Neural Collapse.

Simplex Equiangular Tight Frame (ETF). A simplex ETF matrix $\mathbf{M} = \{\mathbf{m}_c \in \mathbb{R}^d \mid c = 1, 2, \dots, C\}$ composed of C column vectors, each corresponding to a class prototype in \mathbb{R}^d . The matrix is defined as:

$$\mathbf{M} = \sqrt{\frac{C}{C-1}} \mathbf{U} (\mathbf{I}_C - \frac{1}{C-1} \mathbf{J}_C) \quad (1)$$

$$\mathbf{m}_a^\top \mathbf{m}_b = \begin{cases} -\frac{1}{C-1}, & \text{if } a \neq b \\ 1, & \text{otherwise} \end{cases} \quad (2)$$

where $\mathbf{U} \in \mathbb{R}^{d \times C}$ denotes a rotation orthogonal matrix $\mathbf{U}^\top \mathbf{U} = \mathbf{I}_C$. $\mathbf{I}_C \in \mathbb{R}^{C \times C}$ is the identity matrix. $\mathbf{J}_C \in \mathbb{R}^{C \times C}$ is an all-ones matrix. All vectors in the Simplex ETF have equal ℓ_2 norm and identical pair-wise angles.

Variability Collapse (\mathcal{NC}_1). The intra-class variability of final-layer features collapses to zero, meaning that all feature vectors corresponding to the same class converge to their corresponding class mean.

Convergence to Simplex ETF (\mathcal{NC}_2). The class means collapse to the vertices of a simplex ETF, forming a maximally symmetric and equidistant configuration.

Self-Duality (\mathcal{NC}_3). Upon appropriate rescaling, the weights of the final classification layer also collapse to the class means. This results in a self-dual structure, where both the classifier weights and class means share the same simplex ETF structure.

Proposed Method

The discovery and analysis of NC in prior work reveal a promising structure for optimal feature clustering in the latent feature space under ideal training conditions. This insight provides valuable guidance on how to shape the latent feature space when data distributions are imperfect. In this work, we aim to leverage the desirable properties of NC within the challenging multi-label FL setting. An overview of the proposed framework is illustrated in Figure 2.

Label-Aware Disentanglement Module

Multi-label classification involves processing images that may contain multiple objects from different categories. This poses challenges for conventional image classification pipelines, which typically employ global average pooling to produce image-level feature representations. However, such pooled representations are often suboptimal for multi-label tasks because they compress multiple semantic concepts into a single vector, making it difficult to learn distinct, class-specific features in the latent feature space. Additionally, the varying number of labels per image further complicates representation learning and limits a model’s ability to structure and control the learned features effectively.

To address these challenges, we draw inspiration from recent advances in multi-label learning (Liu et al., 2021; Ridnik et al., 2023; Xu et al., 2023), which focus on extracting label-specific features. Building on this idea, we incorporate an attention mechanism to extract class-specific information from the image-level representation, thereby enhancing the discriminative power of each label. In our proposed pipeline, each input image is first processed by a standard feature extractor such as a CNN or transformer to produce a global feature representation. This is then passed to the Label-Aware Disentanglement Module (LADM), which utilises a 4-head cross-attention mechanism to derive label-specific features. In the FL setting, each client trains exclusively on its local data, which often deviates significantly from the global distribution. To address this issue, we adopt a predefined ETF matrix, used both as the classifier and as the source of class-wise query embeddings in LADM. By sharing this fixed query matrix across all clients, LADM ensures a consistent strategy for extracting disentangled, class-specific features during local training. This consistency reduces conflicts during model aggregation and promotes better feature alignment in the global model. The following equations detail the overall process:

$$\begin{aligned} \mathbf{H} &= \text{LADM}(\mathbf{M}, \mathbf{f}) \\ &= \text{Concat}_0 (\text{MultiHeadAttn}(\mathbf{m}_c, \mathbf{f}))_{c=1}^C, \end{aligned} \quad (3)$$

where $\mathbf{f} \in \mathbb{R}^d$ denotes the image-level feature, serving as both the key and value in the attention mechanism. The output $\mathbf{H} \in \mathbb{R}^{C \times d}$ represents the class-specific features generated by LADM. $\mathbf{M} \in \mathbb{R}^{d \times C}$ is a predefined ETF matrix that provides class-wise query embeddings, where \mathbf{m}_c is the query for class c . Concat_0 denotes concatenation along dimension 0.

Neural Collapse-Inspired Feature Alignment

After disentangling image-level features into class-specific representations, each feature captures a distinct semantic concept. This enables the effective adaptation of established representation learning techniques from the multi-class setting to the multi-label context. Rather than allowing each local model to independently learn its own classification boundaries, which can be hindered by label imbalance or missing classes, we fix the classifier using a predefined simplex ETF matrix. This design enforces maximal angular separation between class embeddings, enhancing the model’s ability to distinguish between classes regardless of the local label distribution. By reducing the influence of local label co-occurrence, this approach also helps mitigate divergence between local and global data distributions. Once class-specific features are extracted via LADM, each feature is projected onto its corresponding ETF classifier weight to compute a class-specific logit. These logits are then passed through a sigmoid activation to obtain binary predictions. The model is trained using binary cross-entropy (BCE) loss. The process is formalised as follows:

$$\hat{y}_i^c = \text{Sigmoid}(\mathbf{h}_i^c \cdot \mathbf{m}_c) \quad (4)$$

$$\mathcal{L}_{\text{BCE}} = -\frac{1}{C} \frac{1}{N} \sum_{c=1}^C \sum_{i=1}^N [y_i^c \log(\hat{y}_i^c) + (1 - y_i^c) \log(1 - \hat{y}_i^c)] \quad (5)$$

where $\mathbf{h}_i^c \in \mathbb{R}^d$ denotes the class-specific feature for class c extracted by LADM for the i -th sample, and $\mathbf{m}_c \in \mathbb{R}^d$ represents the fixed ETF classifier weight corresponding to class c . C is the total number of classes, and N denotes the number of training samples available on the client.

Reducing Noise and Improving Clustering

After extracting class-wise features using LADM, each sample is associated with multiple features, corresponding to the total number of classes. Based on the ground-truth labels, a subset of these features is considered as positive, while the remaining ones are treated as negative. To promote more effective clustering in the latent feature space, we introduce two additional regularization terms. These terms are designed to suppress potential noise introduced by negative features and to encourage compact clustering of positive features belonging to the same class.

Negative Feature Rejection Loss: The \mathcal{L}_{BCE} loss encourages each class-wise feature to align with its corresponding ETF prototype if it corresponds to a ground-truth (positive) label, and to be pushed away from its prototype if it corresponds to

a negative label. To further reduce prediction ambiguity, it is important to prevent negative features from aligning with any other class prototypes. To address this, we compute the similarity between negative features and all class-wise prototypes, applying a penalty to high similarity scores. This regularization helps suppress the influence of negative features on the final prediction and mitigates potential noise. The process is formalised as follows:

$$\hat{y}_{ij}^- = \text{Sigmoid}(\mathbf{h}_i^- \cdot \mathbf{m}_j) \quad (6)$$

$$\mathcal{L}_{\text{Neg}} = -\frac{1}{C} \frac{1}{N} \sum_{j=1}^C \sum_{i=1}^N \mathbb{I}(\hat{y}_{ij}^- > \tau) \cdot \log(1 - \hat{y}_{ij}^-) \quad (7)$$

where $\mathbf{h}_i^- \in \mathbb{R}^d$ denotes the negative feature of sample i . The threshold τ is a predefined value used to filter out negative features with low similarity scores, ensuring that only confident negative predictions contribute to the loss. In our experiments, we empirically set $\tau = 0.3$.

Positive Feature Contrastive Loss: To encourage more compact and discriminative class-wise clustering in the latent feature space, we introduce a contrastive loss. This loss enforces positive features to remain close to their corresponding class prototypes while being pushed away from all other class prototypes. The formulation is:

$$\mathcal{L}_{\text{Pos}} = -\frac{1}{N} \sum_{i=1}^N \log \frac{e^{\mathbf{h}_i^c \cdot \mathbf{m}_c}}{\sum_{j=1}^C e^{\mathbf{h}_i^c \cdot \mathbf{m}_j}} \quad (8)$$

where $\mathbf{h}_i^c \in \mathbb{R}^d$ denotes the positive feature of sample i for class c . \mathbf{m}_j represents the predefined prototype for class j .

With the two regularization terms, one designed to suppress noise from negative features and the other to encourage compact clustering of positive features, the total loss can be expressed as:

$$\mathcal{L}_{\text{total}} = \mathcal{L}_{\text{BCE}} + \lambda_1 \mathcal{L}_{\text{Neg}} + \lambda_2 \mathcal{L}_{\text{Pos}} \quad (9)$$

where λ_1 and λ_2 are hyperparameters used to balance the BCE loss and the two regularization terms.

Experiment

Dataset and Evaluation Metric

Datasets: We conduct experiments on both general computer vision (CV) datasets and medical imaging datasets to evaluate the effectiveness and real-world applicability of the proposed method. For general CV tasks, we use CIFAR-10 (Krizhevsky et al., 2009) and PASCAL VOC (Everingham et al., 2010). Since CIFAR-10 is originally a multi-class dataset, we adopt the method used by Li et al. (2023a) to transform it into a multi-label dataset. This is done by merging multiple images into a single composite image, with the combined labels serving as the new ground truth. For medical imaging tasks, we use DermaMNIST (Yang et al., 2023a) and ChestX-ray14 (Wang

et al., 2017). DermaMNIST, which originally contains 7 skin disease categories in a multi-class format, is converted to a multi-label dataset using the same strategy applied to CIFAR-10. ChestX-ray14 is naturally a multi-label dataset, comprising 14 thoracic disease categories and an additional ‘‘No Finding’’ label. Since a significant portion of the dataset, approximately four-sevenths of the training data, are ‘‘No Finding’’ samples (negative cases with all-zero labels), we distribute these samples evenly across all clients. This setup mimics a realistic clinical scenario in which healthy cases are prevalent, while disease cases are relatively rare and unevenly distributed across clients. Detailed information about the datasets and local data distributions under various experimental settings is provided in the Appendix.

Evaluation Metric: Given our focus on label-skewed data distributions, where certain classes may be missing or underrepresented, we report both overall (micro) and class-wise (macro) performance metrics. Following standard practices across different datasets, we report AUC and F1 scores for CIFAR-10, PASCAL VOC, and DermaMNIST, and AUC for ChestX-ray14. Together, these metrics offer a balanced and comprehensive evaluation by capturing both overall performance and class-specific behaviour.

Task Setup and Implementation Details

Task Setup: We simulate the FL system with 10 clients and adopt a full client participation strategy. To reflect the standard heterogeneous FL setting, we introduce non-IID data distributions by partitioning the data using a Dirichlet distribution, parameterised by the concentration factor β . To further emulate label-skewed scenarios, we define a class presence ratio γ , which limits the number of classes available to each client and simulates cases where certain classes are entirely absent from local datasets.

Implementation Details: For all experiments, we use ResNet-18 (He et al., 2016) as the feature extractor. Each FL global model is trained over 100 communication rounds, with one epoch of local training per round. The final model is selected based on its best performance on the validation set. We use a batch size of 32 and initialise the learning rate at 1×10^{-4} , using the AdamW optimiser with a weight decay of 0.01. Models for the CIFAR-10 dataset are trained from scratch, while models for other datasets are initialised with ImageNet-pretrained weights. During training, the regularisation hyperparameter λ_1 is empirically set to either 1 or 0.01, depending on the background complexity of the dataset. For datasets with complex backgrounds, where disentangling class-specific features is more challenging, a smaller value ($\lambda_1 = 0.01$) is used to reduce potential interference with positive feature learning. The other regularisation hyperparameter, λ_2 , is fixed at 1 across all experiments.

Performance Comparison

To evaluate the effectiveness of the proposed method, we compare it with other methods across four datasets, as shown in Ta-

	$\beta = 0.5, \gamma = 0.5$				$\beta = 0.1, \gamma = 0.5$			
	macro-AUC	macro-F1	AUC	F1	macro-AUC	macro-F1	AUC	F1
Centralized (Upperbound)	91.17	61.40	91.04	62.22	91.17	61.40	91.04	62.22
FedAvg (McMahan et al., 2017)	82.46	40.65	81.83	41.24	78.84	31.15	77.00	34.98
FedCurv (Shoham et al., 2019)	82.19	39.36	81.81	39.61	79.03	32.31	77.97	36.13
FedProx (Li et al., 2020)	82.23	39.37	81.68	39.27	79.40	31.01	76.69	35.73
SCAFFOLD (Karimireddy et al., 2020)	82.01	38.41	81.49	38.83	79.29	32.38	77.74	35.90
SphereFed (Dong et al., 2022)	84.85	47.58	85.04	47.29	83.27	39.52	79.45	40.77
FedLGT (Liu et al., 2024)	84.24	45.45	84.16	45.99	81.44	35.95	81.49	38.78
FedNCAIalign-ML (ours)	87.72	49.22	87.13	49.60	84.07	<u>38.14</u>	<u>79.56</u>	42.85

Table 1: Comparisons on the multi-label CIFAR-10 dataset (Krizhevsky et al., 2009). Non-IID data distributions across clients are simulated using the Dirichlet concentration parameter (β) and the class-missing ratio (γ).

	$\beta = 0.5, \gamma = 0.71$				$\beta = 0.1, \gamma = 0.71$			
	macro-AUC	macro-F1	AUC	F1	macro-AUC	macro-F1	AUC	F1
Centralized (Upperbound)	91.86	63.49	94.52	73.30	91.86	63.49	94.52	73.30
FedAvg (McMahan et al., 2017)	90.18	53.96	<u>92.68</u>	67.53	83.95	40.69	86.68	63.03
FedCurv (Shoham et al., 2019)	<u>90.31</u>	56.17	92.64	<u>68.11</u>	<u>86.20</u>	42.19	<u>89.54</u>	64.76
FedProx (Li et al., 2020)	90.16	55.85	92.44	67.95	83.73	42.98	87.96	63.50
SCAFFOLD (Karimireddy et al., 2020)	89.56	54.88	92.13	67.59	85.33	43.60	89.41	<u>64.75</u>
SphereFed (Dong et al., 2022)	85.36	44.25	89.46	53.40	83.37	41.90	88.92	50.94
FedLGT (Liu et al., 2024)	87.33	<u>56.24</u>	90.84	68.25	84.80	<u>44.09</u>	88.70	57.35
FedNCAIalign-ML (ours)	90.42	56.39	92.95	67.78	87.69	51.38	90.36	63.26

Table 2: Comparisons on the multi-label DermaMNIST dataset (Yang et al., 2023a).

	$\beta = 0.05, \gamma = 0.5$				$\beta = 0.01, \gamma = 0.5$			
	macro-AUC	macro-F1	AUC	F1	macro-AUC	macro-F1	AUC	F1
Centralized (Upperbound)	95.66	74.77	96.22	77.15	95.66	74.77	96.22	77.15
FedAvg (McMahan et al., 2017)	93.72	57.00	94.20	64.62	93.29	49.16	93.90	61.08
FedCurv (Shoham et al., 2019)	<u>93.69</u>	57.32	94.40	64.74	<u>93.33</u>	48.93	93.87	61.35
FedProx (Li et al., 2020)	93.70	57.08	<u>94.26</u>	64.46	93.05	48.99	93.74	61.16
SCAFFOLD (Karimireddy et al., 2020)	93.07	58.20	93.97	65.86	93.44	50.89	<u>93.93</u>	62.10
SphereFed (Dong et al., 2022)	85.72	33.71	87.38	38.19	86.85	32.44	87.94	36.18
FedLGT (Liu et al., 2024)	91.07	<u>61.40</u>	91.39	<u>65.88</u>	91.20	<u>56.59</u>	91.20	<u>64.58</u>
FedNCAIalign-ML (ours)	93.82	64.34	94.18	66.42	93.07	62.08	93.95	66.00

Table 3: Comparison of related FL methods with ours on the multi-label PASCAL VOC 2012 dataset (Everingham et al., 2010).

bles 1, 2, 3, and 4. As observed in these tables, our method consistently achieves the best performance in most cases across different datasets. The improvement is particularly notable on naturally long-tailed datasets such as DermaMNIST and ChestX-ray14, where our method yields substantial gains in class-wise performance, indicating its ability to produce more balanced predictions. Specifically, under the $\beta = 0.1$ setting on DermaMNIST, our method outperforms the second-best approach by 1.49% in class-wise AUC and 7.29% in class-wise F1 score. For PASCAL VOC, when each client is limited to a maximum of half the total classes, our method achieves improvements of 2.94% and 5.49% in class-wise F1 score under the $\beta = 0.05$ and $\beta = 0.01$ settings, respectively. For ChestX-ray14 under the $\beta = 0.5$ and $\beta = 0.1$ settings, our method improves class-wise AUC by 0.64% and 1.31%, respectively. Overall, across a range of non-IID configurations with limited class availability per client, our method consistently outperforms existing FL approaches, demonstrating strong robustness to various label-skewed data distributions.

Ablation Study

To evaluate the effectiveness of each component in the proposed method, we conducted an ablation study on the multi-label DermaMNIST dataset, with the client data distribution configured using $\beta = 0.1$ and $\gamma = 0.71$. The experimental results are presented in Table 5. As shown in the table, incorporating LADM for class-specific feature extraction, together with the predefined ETF classifier to encourage class-wise clustering alignment across clients in the latent feature space, yields improvements of 0.43% in class-wise AUC and 7.34% in class-wise F1 score. Additional performance gains are achieved by introducing regularisation terms that enhance the model’s discriminative ability, resulting in further improvements of 3.31% in class-wise AUC and 3.43% in class-wise F1 score.

We also investigated the class-wise query mechanism within the attention-based LADM module. As reported in Table 6, fixed, well-designed class-wise queries consistently outperform learnable queries across most evaluation metrics. This

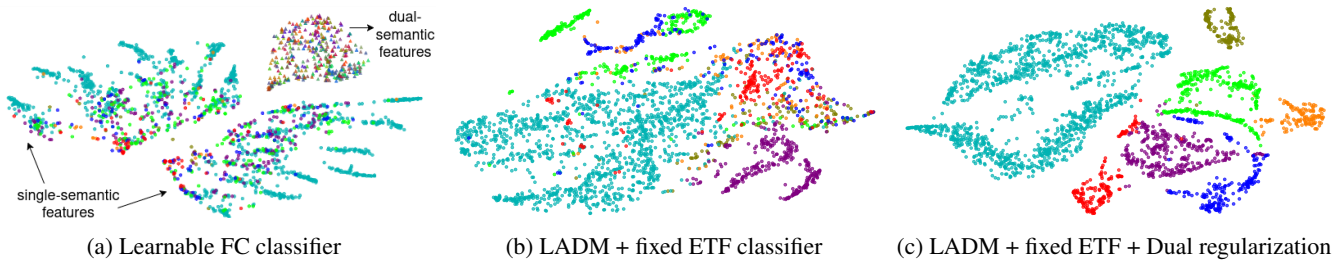


Figure 3: t-SNE visualisation of test data feature embeddings on the multi-label DermaMNIST experiment with $\beta = 0.1$, $\gamma = 0.71$. Each colour represents a class. Observing from subfigure (a), without feature disentanglement (LADM), the model relies on undesired information, such as the number of labels per sample, for clustering.

	$\beta = 0.5, \gamma = 0.5$		$\beta = 0.1, \gamma = 0.5$	
	macro-AUC	AUC	macro-AUC	AUC
Centralized	71.44	79.62	71.44	79.62
FedAvg	69.07	73.28	69.84	78.00
FedCurv	68.12	72.15	69.46	77.63
FedProx	69.23	72.45	69.23	77.69
SCAFFOLD	69.02	72.21	66.71	78.69
SphereFed	57.48	70.26	61.80	74.59
FedLGT	69.76	72.41	70.02	77.93
FedNAlign-ML	70.40	<u>72.62</u>	71.33	<u>78.10</u>

Table 4: Comparison of related FL methods with ours on the ChestX-ray14 dataset (Wang et al., 2017).

ETF Clf	LADM	\mathcal{L}_{Neg}	\mathcal{L}_{Pos}	macro-AUC	macro-F1	AUC	F1
				83.95	40.69	86.68	63.03
✓	✓			84.38	47.95	86.70	60.49
✓	✓	✓		84.73	45.06	89.71	62.89
✓	✓		✓	85.20	49.84	89.03	61.06
✓	✓	✓	✓	87.69	51.38	90.36	63.26

Table 5: Ablation study of the proposed method on the multi-label DermaMNIST dataset with $\beta = 0.1$, $\gamma = 0.71$.

outcome is intuitive in the context of label-skewed FL, where each client has a unique local data distribution. If the queries and classifier are learnable, the model may overfit to these local distributions, which can significantly deviate from the global distribution. Such overfitting introduces inconsistencies among client models and ultimately degrades the performance of the aggregated global model. To maintain consistent learning across clients with non-iid data, it is therefore preferable to use predefined, well-separated, fixed embeddings to guide the learning process rather than relying on learnable representations.

To further analyse model behaviour, we present t-SNE visualisations of feature distributions from the test data in the latent feature space, generated under different model architectures and training strategies on the multi-label DermaMNIST dataset. The client data distribution is configured using $\beta = 0.1$ and $\gamma = 0.71$. As shown in Figure 3, when a conventional, learnable fully connected (FC) classifier is used, although the model achieves 83.95% class-wise AUC

query type	query init	macro-AUC	macro-F1	AUC	F1
learnable	random	82.94	47.94	86.33	57.37
learnable	ETF	85.39	46.92	84.94	53.37
fixed	ETF	84.38	47.95	86.70	60.49

Table 6: Ablation study of the class-wise feature extraction block - LADM on the multi-label DermaMNIST dataset.

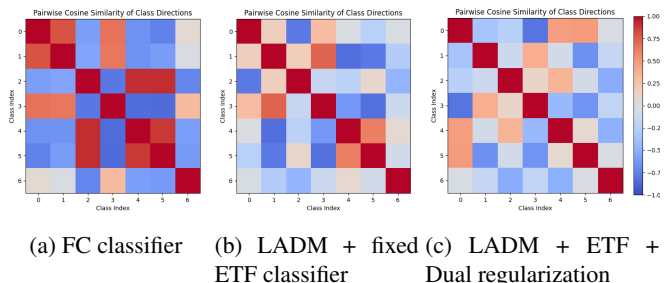


Figure 4: Pair-wise cosine similarity between test data class-wise average feature prototypes.

and 40.69% F1 score, the resulting feature representations exhibit poor clustering. Notably, the model appears to rely on undesired information. Specifically, it tends to group features based on the number of labels per sample, rather than focusing solely on semantic content. By incorporating LADM for extracting single-class features and employing a predefined ETF classifier to regulate feature distribution across clients, the model learns to focus more on semantic content for clustering. This leads to more disentangled, class-specific feature representations and improved clustering quality. Figure 4 also shows that the pairwise cosine similarity between class-wise average features is substantially reduced, indicating enhanced inter-class separability and stronger discriminative capability. Finally, with the addition of extra regularisation terms during training, the feature clustering becomes more compact and semantically coherent, and the similarity among class-wise average prototypes is further reduced.

Conclusion

This paper investigates multi-label label-skewed FL, a practically important yet underexplored problem setting. This task is particularly challenging due to the complexities inherent in multi-label data, combined with difficulties introduced by the federated system, including heterogeneous local data distributions and inconsistencies between local and global data distributions. Inspired by Neural Collapse theory, we propose a feature disentanglement module and incorporate a predefined ETF structure to facilitate the extraction and clustering of class-specific representations, while also aligning feature distributions across clients in the latent feature space. Furthermore, we incorporate specific regularization losses to suppress noisy negative features and enhance compact class-wise clustering. Experiments on four benchmark datasets across eight settings show that our method outperforms existing approaches, with gains of up to 2.87% in class-wise AUC and 7.29% in class-wise F1 score.

Acknowledgments

This work was supported by the UKRI grant EP/X040186/1 (Turing AI Fellowship). This work was also partly supported by the InnoHK-funded Hong Kong Centre for Cerebrocardiovascular Health Engineering (COCHE) Project 2.1 (Cardiovascular risks in early life and fetal echocardiography).

References

- Dong, X., Zhang, S. Q., Li, A., and Kung, H. (2022). Spherefed: Hyperspherical federated learning. In *European Conference on Computer Vision*, pages 165–184. Springer.
- Everingham, M., Van Gool, L., Williams, C. K., Winn, J., and Zisserman, A. (2010). The pascal visual object classes (voc) challenge. *International journal of computer vision*, 88:303–338.
- Gao, J., Zhao, H., dan Guo, D., and Zha, H. (2024). Distribution alignment optimization through neural collapse for long-tailed classification. In *Forty-first International Conference on Machine Learning*.
- Guo, K., Ding, Y., Liang, J., Wang, Z., He, R., and Tan, T. (2025). Exploring vacant classes in label-skewed federated learning. In *Proceedings of the AAAI Conference on Artificial Intelligence*, volume 39, pages 16960–16968.
- He, K., Zhang, X., Ren, S., and Sun, J. (2016). Deep residual learning for image recognition. In *Proceedings of the IEEE conference on computer vision and pattern recognition*, pages 770–778.
- Karimireddy, S. P., Kale, S., Mohri, M., Reddi, S., Stich, S., and Suresh, A. T. (2020). Scaffold: Stochastic controlled averaging for federated learning. In *International conference on machine learning*, pages 5132–5143. PMLR.
- Kirkpatrick, J., Pascanu, R., Rabinowitz, N., Veness, J., Desjardins, G., Rusu, A. A., Milan, K., Quan, J., Ramalho, T., Grabska-Barwinska, A., et al. (2017). Overcoming catastrophic forgetting in neural networks. *Proceedings of the national academy of sciences*, 114(13):3521–3526.
- Krizhevsky, A., Hinton, G., et al. (2009). Learning multiple layers of features from tiny images.
- Lanchantin, J., Wang, T., Ordonez, V., and Qi, Y. (2021). General multi-label image classification with transformers. In *Proceedings of the IEEE/CVF conference on computer vision and pattern recognition*, pages 16478–16488.
- Li, P., Wang, Y., Li, X., and Qu, Q. (2023a). Neural collapse in multi-label learning with pick-all-label loss.
- Li, T., Sahu, A. K., Zaheer, M., Sanjabi, M., Talwalkar, A., and Smith, V. (2020). Federated optimization in heterogeneous networks. *Proceedings of Machine learning and systems*, 2:429–450.
- Li, Z., Shang, X., He, R., Lin, T., and Wu, C. (2023b). No fear of classifier biases: Neural collapse inspired federated learning with synthetic and fixed classifier. In *Proceedings of the IEEE/CVF International Conference on Computer Vision*, pages 5319–5329.
- Liu, I.-J., Lin, C.-S., Yang, F.-E., and Wang, Y.-C. F. (2024). Language-guided transformer for federated multi-label classification. In *Proceedings of the AAAI Conference on Artificial Intelligence*, volume 38, pages 13882–13890.
- Liu, S., Zhang, L., Yang, X., Su, H., and Zhu, J. (2021). Query2label: A simple transformer way to multi-label classification. *arXiv preprint arXiv:2107.10834*.
- McMahan, B., Moore, E., Ramage, D., Hampson, S., and y Arcas, B. A. (2017). Communication-efficient learning of deep networks from decentralized data. In *Artificial intelligence and statistics*, pages 1273–1282. PMLR.
- Papayan, V., Han, X., and Donoho, D. L. (2020). Prevalence of neural collapse during the terminal phase of deep learning training. *Proceedings of the National Academy of Sciences*, 117(40):24652–24663.
- Radford, A., Kim, J. W., Hallacy, C., Ramesh, A., Goh, G., Agarwal, S., Sastry, G., Askell, A., Mishkin, P., Clark, J., et al. (2021). Learning transferable visual models from natural language supervision. In *International conference on machine learning*, pages 8748–8763. PmLR.
- Ridnik, T., Sharir, G., Ben-Cohen, A., Ben-Baruch, E., and Noy, A. (2023). MI-decoder: Scalable and versatile classification head. In *Proceedings of the IEEE/CVF winter conference on applications of computer vision*, pages 32–41.

- Shoham, N., Avidor, T., Keren, A., Israel, N., Benditkis, D., Mor-Yosef, L., and Zeitak, I. (2019). Overcoming forgetting in federated learning on non-iid data. *arXiv preprint arXiv:1910.07796*.
- Tao, Z., Li, S.-Y., Wan, W., Zheng, J., Chen, J.-Y., Li, Y., Huang, S.-J., and Chen, S. (2025). Mlc-nc: Long-tailed multi-label image classification through the lens of neural collapse. In *Proceedings of the AAAI Conference on Artificial Intelligence*, volume 39, pages 20850–20858.
- Wang, X., Peng, Y., Lu, L., Lu, Z., Bagheri, M., and Summers, R. M. (2017). Chestx-ray8: Hospital-scale chest x-ray database and benchmarks on weakly-supervised classification and localization of common thorax diseases. In *Proceedings of the IEEE Conference on Computer Vision and Pattern Recognition (CVPR)*, pages 3462–3471.
- Wei, K., Xu, Z., and Deng, C. (2025). Compress to one point: Neural collapse for pre-trained model-based class-incremental learning. In *Proceedings of the AAAI Conference on Artificial Intelligence*, volume 39, pages 21465–21473.
- Xu, P., Xiao, L., Liu, B., Lu, S., Jing, L., and Yu, J. (2023). Label-specific feature augmentation for long-tailed multi-label text classification. In *Proceedings of the AAAI conference on artificial intelligence*, volume 37, pages 10602–10610.
- Yang, J., Shi, R., Wei, D., Liu, Z., Zhao, L., Ke, B., Pfister, H., and Ni, B. (2023a). Medmnist v2-a large-scale lightweight benchmark for 2d and 3d biomedical image classification. *Scientific Data*, 10(1):41.
- Yang, Y., Yuan, H., Li, X., Lin, Z., Torr, P., and Tao, D. (2023b). Neural collapse inspired feature-classifier alignment for few-shot class incremental learning. *arXiv preprint arXiv:2302.03004*.

Appendix

Pseudo Code for FedNCAAlign-ML

We present the pseudocode for our proposed FedNCAAlign-ML in Algorithm 1. The input comprises a set of clients, each with its own local dataset, and a centralized server responsible for managing communication. The training process involves three iterative steps: local training on client devices, aggregation at the central server, and broadcasting the updated global model back to the clients. While we adopt the standard FL protocol for aggregation and broadcasting, the core contribution of FedNCAAlign-ML lies in its specialized model design and the local training procedure tailored for multi-label label-skewed FL scenarios. During local training, each client first encodes its input data using a standard feature extractor to generate image-level representations. These representations are then passed to the proposed Label Aware Disentanglement Module (LADM), which produces disentangled, class-wise embeddings. By capturing distinct semantic concepts within each feature, these embeddings facilitate more effective and controllable clustering in the latent feature space. To further enhance consistent and discriminative feature alignment across clients, particularly under label-skewed conditions, we introduce a shared, predefined Equiangular Tight Frame (ETF) structure. This structure encourages class-independent clustering and aligns local features with a global class geometry, helping to mitigate overfitting to local data distributions. Additionally, two complementary regularization terms are introduced to enhance feature clustering in the latent feature space: a rejection loss to filter out noisy signals from negative features, and a contrastive loss to promote compact intra-class clustering and clear inter-class separation.

Algorithm 1: Federated Neural Collapse Alignment for Multi-Label Learning (FedNCAAlign-ML)

Input: K clients; local datasets $\{\mathcal{D}_k\}_{k=1}^K$; initial global parameters w_0 ; predefined ETF matrix M ; learning rate η ; local epochs E .

```

1: Server:
2: Initialize  $w \leftarrow w_0$ 
3: for  $t = 0$  to  $T$  do ▷  $t$ -th communication round
4:   for each client  $k = 1, \dots, K$  in parallel do
5:      $w_{t+1}^k \leftarrow \text{CLIENTUPDATE}(\mathcal{D}_k, w_t)$ 
6:     Send the client model  $w_{t+1}^k$  to the server
7:   end for
8:    $w_{t+1} \leftarrow \text{MODELAGGREGATION}(\{w_{t+1}^k\}_{k=1}^K)$ 
9:   Broadcast the global model  $w_{t+1}$  to all clients
10: end for

11: ClientUpdate( $\mathcal{D}_k, w$ ):
12: Split  $\mathcal{D}_k$  into batches  $\{b\}$ 
13: for  $e = 0$  to  $E$  do ▷  $e$ -th local epoch
14:   for each batch  $b$  in  $\{b\}$  do
15:     Extract inputs  $(x, y)$  from  $b$ 
16:      $\mathbf{f} \leftarrow \text{FeatureExtractor}(w; x)$ 
17:      $\mathbf{H} \leftarrow \text{LADM}(M, \mathbf{f})$  ▷ Eq. 3
18:     Compute loss  $\mathcal{L}_{\text{total}}(w; M, \mathbf{H})$  ▷ Eqs. 5, 7, 8, 9
19:      $w \leftarrow w - \eta \nabla_w \mathcal{L}_{\text{total}}$ 
20:   end for
21: end for
22: Return  $w$ 

```

Ablation Study (additional)

To complement the results reported in the main manuscript, we present an additional ablation study to evaluate the contribution of each component in our proposed method. The experiments are conducted on the multi-label CIFAR-10 dataset (Krizhevsky et al., 2009), with the client data distribution configured using a Dirichlet concentration parameter $\beta = 0.5$ and a class-presenting ratio $\gamma = 0.5$. The experimental results are summarized in Tables 7 and 8, and Figures 5 and 6. As shown in Table 7, integrating LADM for class-specific feature extraction, along with the use of a predefined ETF classifier to encourage class-wise clustering alignment across clients in the latent feature space, leads to performance improvements of 3.38% in class-wise AUC and 3.99% in class-wise F1 score. Additional gains are achieved by introducing regularization terms that enhance the model’s discriminative capacity, resulting in a further class-wise increase of 1.88% in AUC and 4.58% in F1 score. Regarding LADM specifically, the results in Table 8 demonstrate that using fixed, well-designed class-wise queries is generally more effective than learnable queries across most evaluation metrics.

To further analyze model behavior, we visualize the latent feature distributions of the test set using t-SNE under different architectural and training configurations. As shown in Figure 5, incorporating LADM for extracting single-class features, along with a predefined ETF classifier to regulate feature distribution across clients, enables the model to focus on semantic content rather than irrelevant factors such as the number of labels per sample. Furthermore, the addition of regularization terms during training leads to more compact and semantically coherent clusters, while also reducing the similarity among class-wise average prototypes. As shown in Figure 6, the pairwise cosine similarity between class-wise average features decreases with the inclusion of LADM and the ETF classifier, and is further reduced by the added regularization terms, indicating enhanced inter-class separability and stronger discriminative capability.

ETF	Cif	LADM	\mathcal{L}_{Neg}	\mathcal{L}_{Pos}	macro-AUC	macro-F1	AUC	F1
					82.46	40.65	81.83	41.24
✓		✓			85.84	44.64	85.10	45.45
✓		✓	✓		87.72	48.22	86.16	48.93
✓		✓		✓	86.78	44.46	86.08	45.28
✓		✓	✓	✓	87.72	49.22	87.13	49.60

Table 7: Ablation study of the proposed method on the multi-label CIFAR10 dataset. β is set to 0.5 and γ is set to 0.5.

Experiments (additional)

To complement the results reported in the main manuscript and further validate the reproducibility of our method, we present additional experiments on the multi-label CIFAR-10 dataset (Krizhevsky et al., 2009). These experiments were repeated three times with different random seeds to evaluate the

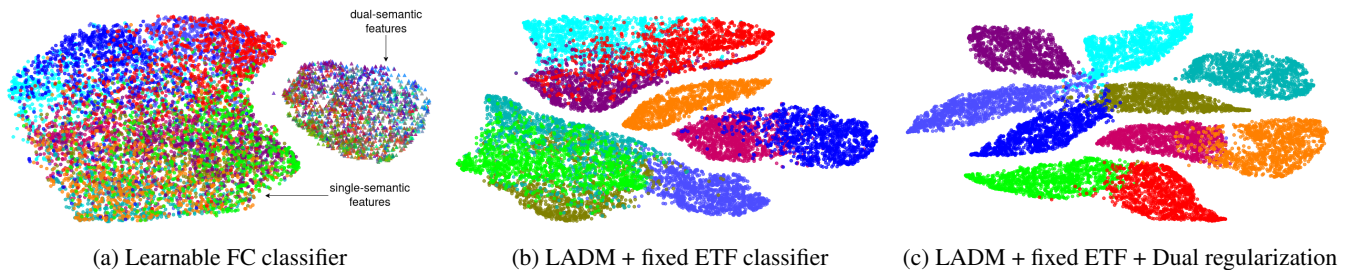


Figure 5: t-SNE visualisation of test data feature embeddings on the multi-label CIFAR10 experiment with $\beta = 0.5, \gamma = 0.5$. Each colour represents a class. Observing from subfigure (a), without feature disentanglement (LADM), the model appears to rely on undesired information, such as the number of labels per sample, for clustering.

query type	query init	macro-AUC	macro-F1	AUC	F1
learnable	random	84.15	38.10	83.70	39.30
learnable	ETF	86.26	43.61	85.41	43.87
fixed	ETF	85.84	44.64	85.10	45.45

Table 8: Ablation study of the class-wise feature extraction block - LADM on the multi-label CIFAR10 dataset.

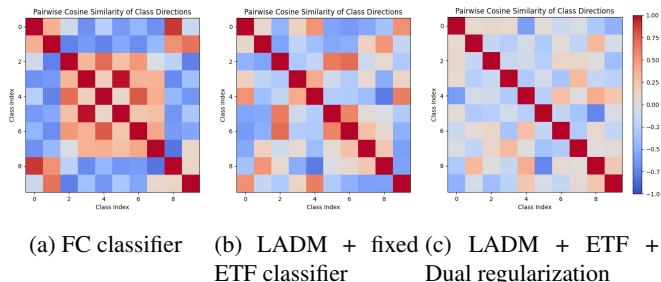


Figure 6: Pair-wise cosine similarity between test data class-wise average feature prototypes on the multi-label CIFAR10 dataset.

stability and effectiveness of the proposed approach. The mean and standard deviation of the results are reported in Table 9. As shown in the table, the proposed method demonstrates stable performance across multiple runs and consistently outperforms competing approaches.

Dataset

In this section, we introduce the datasets used in our experiments. To evaluate both the effectiveness and real-world applicability of the proposed method, we conduct experiments on datasets from general computer vision (CV) as well as medical imaging domains. Specifically, we use CIFAR-10 (Krizhevsky et al., 2009) and PASCAL VOC (Everingham et al., 2010) as general CV datasets, and DermaMNIST (Yang et al., 2023a) and ChestX-ray14 (Wang et al., 2017) as medical datasets. We simulate the FL system with 10 clients. To model non-IID data distributions, the data is partitioned using a Dirichlet distribution, with the concentration parameter β controlling the degree of heterogeneity. To further simulate missing-class scenarios, we constrain the number of classes available to each client us-

ing the class-presenting ratio γ , which specifies the proportion of total classes present locally. Dataset-specific settings are detailed below.

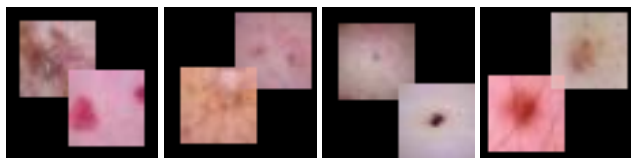
CIFAR-10 (Krizhevsky et al., 2009) is a widely used benchmark in CV. It comprises 10 classes: *airplane, automobile, bird, cat, deer, dog, frog, horse, ship, and truck*. To adapt CIFAR-10 for multi-label classification, following Li et al. (2023a), we create composite samples by combining multiple original images into a single image, with their corresponding labels forming a multi-label ground truth. Specifically, we retain a portion of the original single-label images and augment the dataset by creating an equal number of synthetic samples for each possible pairwise class combination. These composites are constructed by randomly selecting two images from different classes and combining them into one. We evaluate our method on the multi-label CIFAR-10 dataset under two FL configurations, using $\beta = 0.5, \gamma = 0.5$ and $\beta = 0.1, \gamma = 0.5$. Figure 8 illustrates the corresponding class-wise data distribution across clients.

DermaMNIST (Yang et al., 2023a) is a skin lesion classification dataset. It consists of 7 diagnostic categories: *actinic keratoses, basal cell carcinoma, benign keratosis-like lesions, dermatofibroma, melanocytic nevi, melanoma, and vascular lesions*. To adapt DermaMNIST for multi-label classification, we apply a strategy similar to the one used for multi-label CIFAR-10. Given the long-tailed nature of the original dataset, we preserve its inherent distribution by retaining all single-label samples. Then, we augment the dataset with an equal number of synthetic samples for each possible pairwise label combination. Figure 7 shows examples of the resulting composite multi-label inputs. The resulting dataset comprises the complete set of original samples along with the newly generated multi-label samples. We evaluate our method on this multi-label DermaMNIST dataset under two FL configurations: $\beta = 0.5, \gamma = 0.71$ and $\beta = 0.1, \gamma = 0.71$. The corresponding class-wise data distributions across clients are illustrated in Figure 9.

PASCAL VOC 2012 (VOC) (Everingham et al., 2010) is a widely used benchmark dataset in CV. It consists of approximately 11,500 images, each annotated with one or more object categories selected from a predefined set of 20 classes. These object categories are: *aeroplane, bicycle, bird, boat, bottle, bus, car, cat, chair, cow, dining table, dog, horse, motorbike,*

	$\beta = 0.5, \gamma = 0.5$			
	macro-AUC	macro-F1	AUC	F1
Centralized (Upperbound)	92.20 \pm 0.36	61.30 \pm 0.94	90.04 \pm 0.65	62.02 \pm 0.62
FedAvg (McMahan et al., 2017)	82.29 \pm 0.46	39.47 \pm 1.59	81.48 \pm 0.78	40.26 \pm 1.09
FedCurv (Shoham et al., 2019)	82.53 \pm 0.30	39.96 \pm 1.28	82.10 \pm 0.29	40.34 \pm 1.04
FedProx (Li et al., 2020)	82.45 \pm 0.34	39.22 \pm 0.74	81.77 \pm 0.48	39.66 \pm 0.53
SCAFFOLD (Karimireddy et al., 2020)	82.51 \pm 0.44	39.98 \pm 1.41	82.08 \pm 0.53	40.26 \pm 1.26
SphereFed (Dong et al., 2022)	83.63 \pm 1.50	42.58 \pm 3.20	83.50 \pm 1.87	43.18 \pm 2.34
FedLGT (Liu et al., 2024)	83.52 \pm 0.68	43.60 \pm 1.68	83.36 \pm 0.71	44.03 \pm 1.71
FedNCAIalign-ML (ours)	87.55 \pm 0.31	49.17 \pm 1.65	87.00 \pm 0.31	49.61 \pm 1.64

Table 9: Comparisons on the multi-label CIFAR-10 dataset (Krizhevsky et al., 2009). Non-IID data distributions across clients are simulated using the Dirichlet concentration parameter (β) and the class-missing ratio (γ).



(a) actinic keratosis, vascular lesions (b) basal cell carcinoma, matrifibroma (c) bird, vascular lesions (d) dermatofibroma, melanoma

Figure 7: Examples from the multi-label DermaMNIST dataset. Each subfigure displays a composite image along with its corresponding set of labels.

person, potted plant, sheep, sofa, train, and TV monitor. This dataset poses a challenging multi-label classification problem due to the presence of class imbalance, intra-class variability, and frequent inter-class co-occurrence. For example, the *person* category often co-occurs with many other object classes. Under a label-skewed FL setting, the non-IID distribution of data and inconsistencies in class co-occurrence patterns across clients further exacerbate the learning difficulty. We evaluate our method on VOC under two FL configurations, using $\beta = 0.05, \gamma = 0.5$ and $\beta = 0.01, \gamma = 0.5$. Figure 10 illustrates the resulting class-wise data distribution across clients.

ChestX-ray14 (Wang et al., 2017) is a large-scale medical imaging dataset commonly used for automated thoracic disease classification. It consists of 112,120 frontal-view chest X-ray images collected from 30,805 unique patients. Each image is annotated with one or more disease labels, making the dataset naturally suitable for multi-label classification tasks. These labels were extracted from corresponding radiology reports using natural language processing techniques. The dataset includes 14 disease categories: *Atelectasis, Cardiomegaly, Consolidation, Edema, Effusion, Emphysema, Fibrosis, Hernia, Infiltration, Mass, Nodule, Pleural Thickening, Pneumonia, and Pneumothorax*. In addition, a *No Finding* label is used to indicate negative samples in which none of the 14 diseases are present. Due to its scale, real-world variability, and label noise, ChestX-ray14 provides a challenging benchmark for developing and evaluating deep learning models in medical image analysis, particularly in multi-label, imbalanced scenarios. We conduct experiments under two label-

skewed FL settings on this dataset, using configurations of $\beta = 0.5, \gamma = 0.5$ and $\beta = 0.1, \gamma = 0.5$. Since a significant portion of the dataset is “No Finding” samples, we distribute these evenly across all clients in both settings. This setup mimics realistic clinical scenarios where healthy cases are common, while disease cases are relatively rare and unequally distributed across institutions. Figure 11 shows the class-wise data distribution across clients.



Figure 8: Distribution of data across local clients used in the experiments on the CIFAR-10 dataset (Krizhevsky et al., 2009).

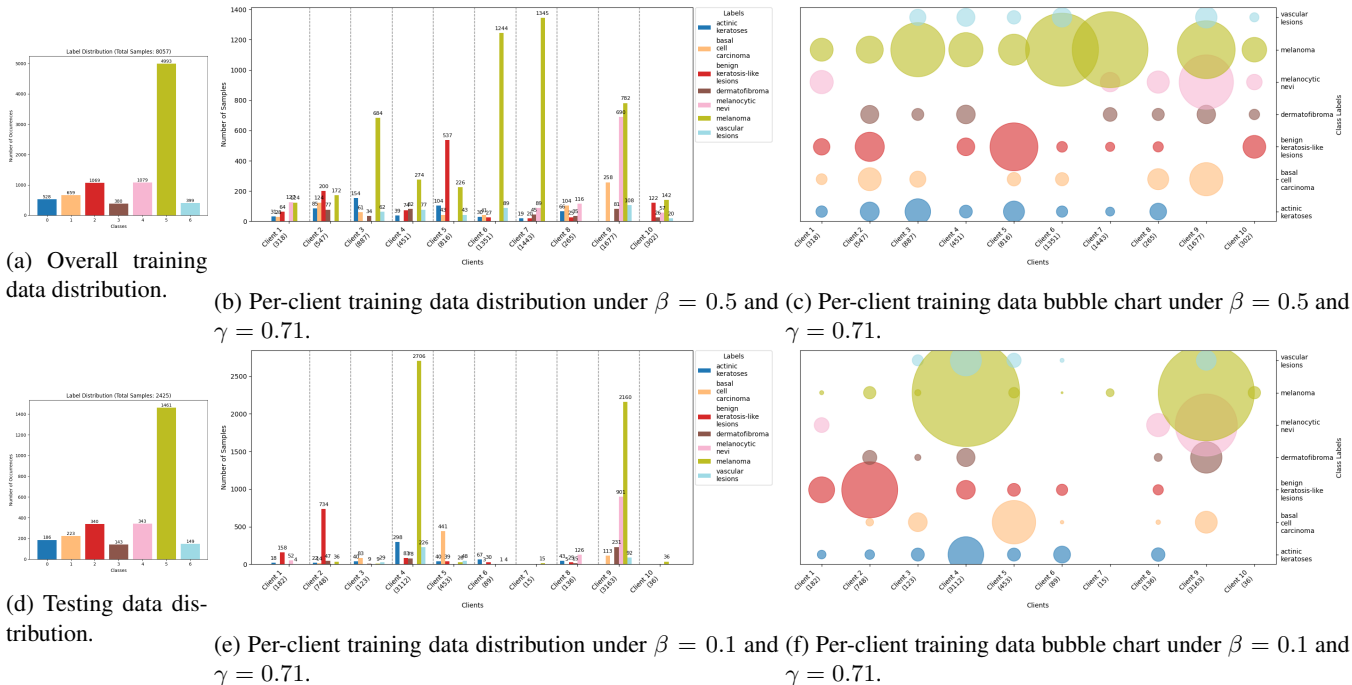


Figure 9: Distribution of data across local clients used in the experiments on the DermaMNIST dataset (Yang et al., 2023a).



Figure 10: Distribution of data across local clients used in the experiments on the VOC dataset (Everingham et al., 2010).

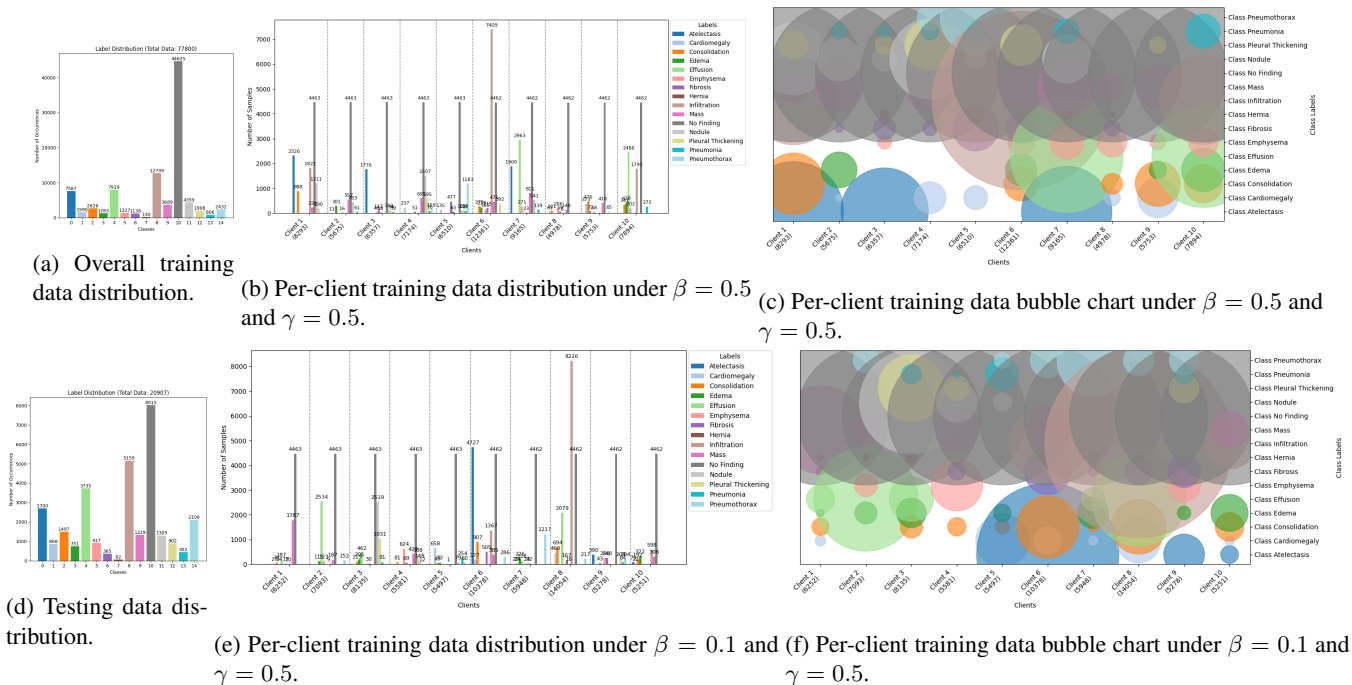


Figure 11: Distribution of data across local clients used in the experiments on the ChestX-ray14 dataset (Wang et al., 2017).